
Self-calibration of rotary axis and linear axes error motions by an automated on-machine probing test cycle

Nico Zimmermann · Soichi Ibaraki

Received: date / Accepted: date

Abstract Efficient, precise and automated in-process calibration schemes are essential to improve the accuracy and productivity of five-axis machine tools. This paper presents a new calibration approach, which combines an on-machine measurement cycle and self-calibration techniques, to evaluate the position errors and the error motions of a rotary axis using a touch trigger probe and an uncalibrated cylindrical artefact. This significantly reduces the downtime of machine tools required for the calibration process. In contrast to many common calibration strategies for rotary axes of five-axis machine tools, the presented self-calibration concept does not neglect the positioning errors of the linear axes when identifying the position errors and the error motions of the rotary axis. The self-calibration procedure is able to separate the positioning errors of the linear axes in radial direction, the radial error motions and the position errors of a rotary axis, as well as the errors related to the uncalibrated artefact. This error separation is realized by a test cycle consisting of four tests in which the measurements are conducted by particular axis movements. Furthermore, the uncertainty analysis of the self-calibration concept is conducted to visualize

the uncertainty propagation within the mathematical model. The self-calibration procedure is analysed by an experimental evaluation, which includes a comparison between the results of the self-calibration approach and an R-Test. This comparison shows that the results of both measurement procedures are consistent.

Keywords Five-axis machine tool · Touch trigger probe · Error calibration · Geometric error · Self-calibration · Error separation

1 Introduction

Five-axis machine tools are characterized by a high productivity for complex workpieces, because the reclamping effort is drastically reduced. Therefore, they are essential in industrial application and precision manufacturing. However, due to the two additional rotary axes, five-axis machine tools have a more complex kinematic chain compared to three-axis machine tools. Consequently, it is challenging to ensure an accurate relative movement between the workpiece and the tool. Direct and indirect measurement approaches have been designed to estimate and calibrate the geometrical errors of five-axis machine tools [13]. In order to realize an efficient calibration of five axis machine tools many indirect calibration approaches such as the R-Test [25], double ball bar tests [27,16] and test piece machining procedures [12,26] have been developed. These approaches are based on multi axes movements and specific mathematical models to identify the considered geometrical errors. Therefore, they do not require to identify each error parameter separately as in the direct calibration approaches.

In recent years, touch trigger probes are frequently used as measurement devices in order to improve effi-

N. Zimmermann
Institute of Machine Tools and Manufacturing (IWF),
ETH Zürich,
Leonhardstrasse 21,
8092 Zürich,
Switzerland
E-mail: zimmermann@iwf.mavt.ethz.ch

S. Ibaraki
Department of Mechanical Systems Engineering,
Hiroshima University,
Kagamiyama 1-4-1,
Higashi-Hiroshima 739-8527,
Japan
E-mail: ibaraki@hiroshima-u.ac.jp

ciency and automation of calibration strategies for five-axis machine tools. Touch trigger probes are available by default on most five-axis machine tools. These calibration methods utilize precision spheres [5, 19], cubic artefacts [11, 10] or the machine table itself [23, 20] as measurement artefact, which is analysed by the touch trigger probe. The common principle of these schemes is to measure the displacement of the Tool Centre Point (TCP) relative to the rotary table, on which the artefact is fixed, at a set of certain angular positions of the two rotary axes. To perform this measurement, the works [5, 19, 11, 10, 23, 20] drive both a rotary and linear axes in combination to identify the relative displacement between the workpiece and the TCP by keeping their distance small (in probing-based schemes or the R-Test) or nominally constant (in the ball bar tests). Consequently, not only the rotary axis but also the linear axes influence the measured displacements. Therefore, the separation of rotary and linear axis' error motions is a challenge. Frequently, assumptions such as neglecting the linear axes related errors are made to avoid the error separation. This issue is also common in the R-Test, double ball bar tests, and test piece machining tests and results in an increased overall calibration uncertainty as described by Bringmann and Knapp [4]. Other approaches realize the separation of the error sources by using a kinematic model based on homogeneous transformation matrices and a numerical optimization [23, 20, 3]. For example, an on-machine calibration procedure developed by Mayer et al. [20] allows to identify errors associated with linear axes in addition to the geometric errors of the rotary axes. However, they are limited to squareness errors between the linear axes and relative positioning error gain between two linear axes. In Rahman and Mayer [23] the position and orientation errors as well as the error motions of a five-axis machine tool are determined by using a touch trigger probe and a machine table equipped with a reference length as artefact. However, this results in a measurement time of 2 h 41 min and they do not present a complete uncertainty analysis including the uncertainty propagation within the mathematical model when the geometric accuracy of the artefact is not ensured. Therefore, further developments to combine on-machine measurement cycles and efficient error separation techniques are essential for a precise and fast calibration of machine tools.

High precision measurement methodologies, including coordinate measurement machines (CMM) [22, 21, 24], spindle [17, 18], roundness [7] and gear measurement procedures [9, 15], often use error separation and self-calibration techniques to separate the errors of the artefact and the measurement device. Self-calibration procedures provide an accurate measurement result with-

out using externally calibrated artefacts. A review of the fundamental theory of self-calibration can be found in [6]. In the field of gear measurement, Guenther et al. [9] developed a method for the self-calibration of a ball plate artefact on a coordinate measuring machine (CMM). This method relies on the Rosette method, which is presented in [15] and is able to separate the errors of the artefact and the used CMM. The approach can separate the error contributions of the artefact, the linear axes and the rotary axes in radial direction. Wang et al. [24] present a method to separate the error motions of a rotary table from the linear axes of the CMM by using a similar ball plate artefact as in [9] and a specific sequence of three Rosette method procedures. This calibrates the rotary table, the 3-axis measurement device and the artefact simultaneously. However, this error separation strategy uses a circular ball artefact, which has to be mounted on the machine tool table to separate the influences of the different error sources.

The calibration procedure presented in this paper combines self-calibration techniques which are mainly used in the field of high precision measurements, with an on-machine measurement cycle to realize an efficient error separation without requiring a complicated measurement setup and a long measurement time. The proposed calibration scheme can separate the linear and rotary axis error motions while conventional schemes neglect linear axes error motions. Additionally, the proposed calibration approach can be fully automated, including the loading and unloading of the test piece and the probe, when the test piece's geometry is only roughly known. Furthermore, any test piece, e.g. the blank part before being machined, can be used and there is no need to keep an artefact with a calibrated geometry. Thus, this approach can be used for regular performance checks of five-axis machine tools before machining high-precision parts without triggering a long downtime. An explicit and efficient calibration approach for rotary axis including an effective error separation is especially required in the case of large machine tools. On large machine tools, for example environmental changes often initially influence the linear axis error motions, which can subsequently influence the calibration result of rotary axis' position errors in the machine coordinate system. Conventional calibration schemes without error separation techniques cannot clearly observe such errors [4].

In Section 2 of this paper the concept and the mathematical model of the new self-calibration approach, which allows to the position errors and the error motions of a rotary axis as well as the positioning error of the linear axes in radial direction by an on-machine measurement cycle, are introduced. An exper-

imental case study of the proposed self-calibration procedure is presented in Section 3. The uncertainty analysis, which is based on a Monte Carlo simulation of the self-calibration approach, is described in Section 4. Section 5 illustrates an extended experimental evaluation including a comparison with a conventional measurement procedure. To close the paper, a conclusion is given in Section 6.

2 Concept of the self-calibration approach

The presented self-calibration approach determines the position errors and the radial error motions of a rotary axis. The method separates the rotary axis related errors from the influence of the positioning errors of the linear axes in radial direction as well as the artefact related errors. The methodology of the self-calibration approach includes four different tests. In each of these tests, a specific combination of the considered axes is moved to arrive at the different measurement positions and ensure a separation of the relevant error sources. The error separation strategy allows to use an uncalibrated cylindrical artefact such as a workpiece or the rotary table for the measurement cycle. This decreases the downtime of the machine tool, because no specific measurement setup is required. The following sections explain the self-calibration approach by means of a workpiece as artefact.

2.1 Error variables to be identified

The objective of the proposed self-calibration approach is to identify four error variables that describe the influence of the different error sources on the measurement results. Table 1 describes these error variables. Figure 1 shows the machine tool configuration that is investigated in this paper.

The measurements of the self-calibration approach are conducted in radial direction with respect to the used artefact. Thus, only the radial displacements resulting from the total error motions of the rotary axis as well as the errors of the linear axes and the artefact are detected. With $E_{XC,total}(C_i)$ and $E_{YC,total}(C_i)$, it is possible to determine the position errors of the rotary axis E_{X0C} and E_{Y0C} in the defined coordinate system as well as the pure radial error motions (E_{XC} and E_{YC}). The position errors of the rotary axis can be calculated using the least-squares circle centre according to ISO 230-7:2015 [2].

For the mathematical description of the self-calibration approach, two coordinate systems are defined. One coordinate system, called the machine coordinate system,

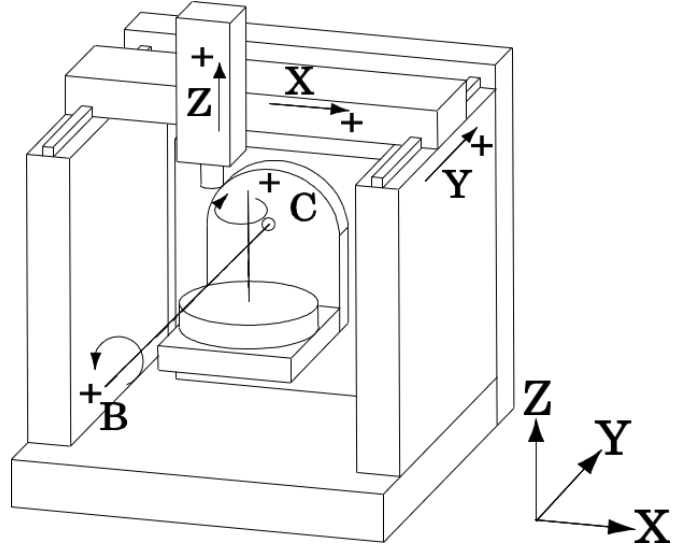


Fig. 1 Configuration of the machine tool under investigation.

Table 1 Definition of the error variables.

Variable name	Description
$E_{XC,total}(C_i)$	Superposition of the influence of the rotary axis' position error, E_{X0C} , and the radial error motion, E_{XC} , in the X- direction as a function of the rotation angle C_i .
$E_{YC,total}(C_i)$	Superposition of the influence of the rotary axis' position error, E_{Y0C} , and the radial error motion, E_{YC} , in the Y- direction as a function of the rotation angle C_i .
$E_{radial,XY}(\theta_i)$	Positioning error of the linear axes in radial direction at the angular position θ_i . $E_{radial,XY}(\theta_i) = EXX(\theta_i) \cdot \cos(\theta_i) + EYY(\theta_i) \cdot \sin(\theta_i)$ Where EXX respectively EYY is the 2D positioning error of the X- and the Y- axis when they are positioned at $(R \cdot \cos(\theta_i), R \cdot \sin(\theta_i))$.
$W_{radial}(\theta_i)$	Shape deviation of the workpiece in the radial direction at the angular position θ_i . It includes the influence of the setup position error of the workpiece with respect to the origin of the machine coordinate system.

has a constant position with respect to the machine tool, the other coordinate system, called the workpiece coordinate system, rotates with the workpiece. The origins of both coordinate systems are located at the nominal position of the C-axis. The Z- position of the origin can be set arbitrarily, since this paper only considers the errors in the XY-plane. Therefore, all measurements of the self-calibration approach are conducted at the same

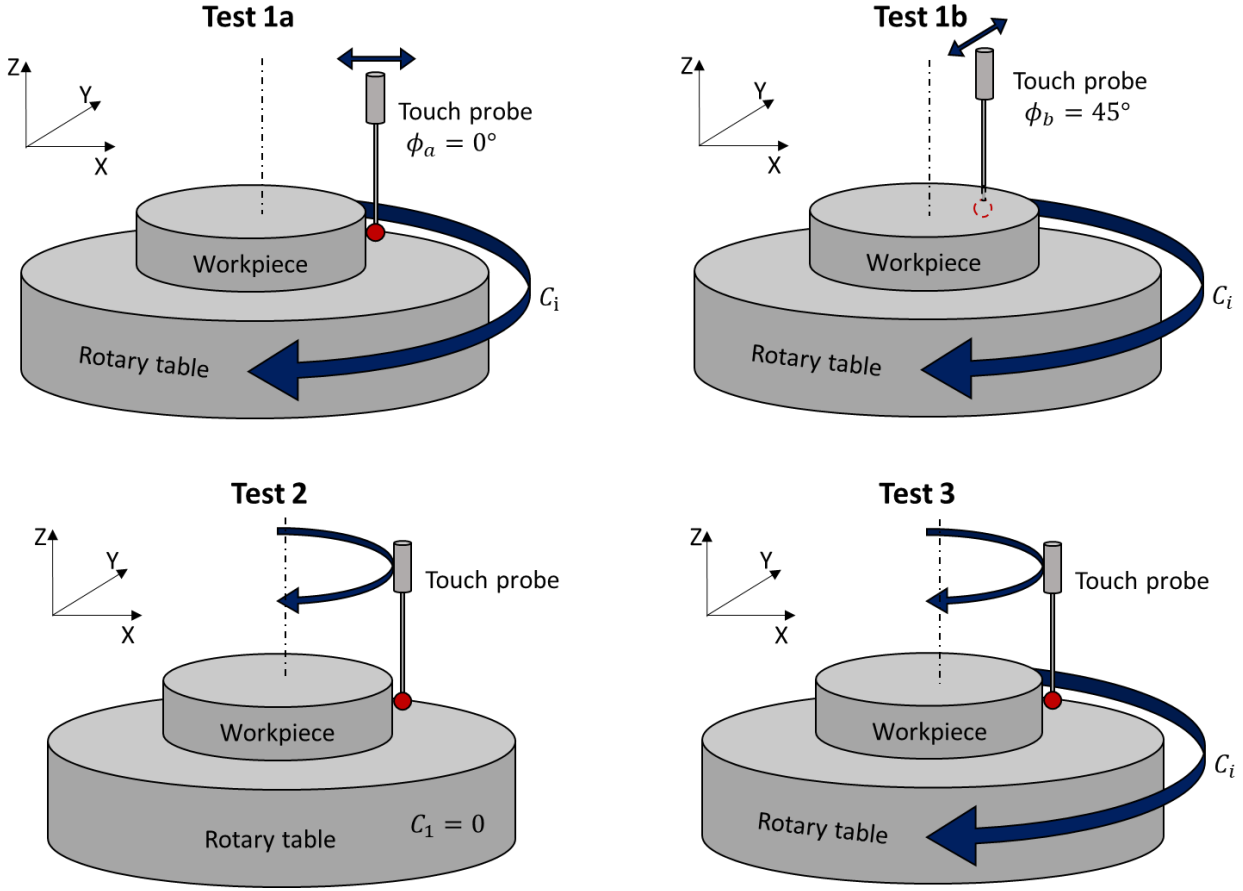


Fig. 2 Combination of the axis movements during the different tests composing the measurement cycle of the self-calibration approach a) Test 1a, b) Test 1b, c) Test 2, d) Test 3.

height and it is not possible to obtain the orientation errors E_{A0C} and E_{B0C} and the angular error motions E_{AC} and E_{BC} of the rotary axis. Consequently, the rotary axis related errors identified by the self-calibration approach depend on the Z- position at which the measurements are conducted. $E_{XC,total}(C_i)$, $E_{YC,total}(C_i)$ and $E_{radial,XY}(\theta_i)$ are described in the machine coordinate system and $W_{radial}(\theta_i)$ is defined in the workpiece coordinate system. The rotation of the C-axis is positive in clockwise direction. The angular positions θ_i of $E_{radial,XY}(\theta_i)$ and $W_{radial}(\theta_i)$ are positive in counter-clockwise direction in its respective coordinate system.

2.2 Proposed test procedure

Figure 2 introduces the measurement procedure consisting of the four different tests, which are developed for the self-calibration approach to separate the influence of the different error sources. During each test, the artefact is touched in radial direction at the defined angular positions. The radius of the uncalibrated artefact is assumed to be unknown. Therefore, the first measure-

ment in the test cycle along the X-axis is the reference for all other measurements.

In Test 1a and Test 1b the rotary axis is turned to reach the measurement positions which are uniformly distributed around the circumference of the artefact. The touch trigger probe is always located at the same position. During Test 1a the touch trigger probe is placed along the X-axis, which is the position $\phi_a = 0^\circ$, of the machine coordinate system. Test 1b differs from Test 1a, because the touch trigger probe is placed at the angular position ϕ_b instead of ϕ_a . In Test 1b the touch trigger probe is located at $\phi_b = 45^\circ$ to capture additionally the effect of $E_{YC,total}(C_i)$. In contrast to Test 1a and Test 1b, in Test 2 only the linear axes X and Y are moved to reach the different measurement positions. The rotary table is fixed at $C_1 = 0^\circ$ during this test. Consequently, the measurement results of Test 2 are not affected by the rotary axis related errors and the measurement results are only influenced by the linear axes and the workpiece errors. The purpose of Test 3 is to measure the radial displacements without the influence of the workpiece related errors. Therefore,

the touch trigger probe touches approximately the same point of the workpiece at each measurement position. Consequently, the rotary axis and the linear axes move simultaneously in order to reach the different measurement positions.

2.3 Algorithm to identify the error variables

In Tests 1a and 1b, the position errors and the radial error motions of the rotary axis, and the workpiece errors at each considered angular position influence the measurement results. The positioning errors of the linear axes in radial direction do not vary at the different measurement positions because the touch trigger probe is always located at the same position. Equation (1) presents the mathematical formulation for Test 1a and Test 1b.

$$r_{1a/b}(C_i) - r_{1a}(0^\circ) = \begin{bmatrix} E_{XC,total}(C_i) \\ E_{YC,total}(C_i) \end{bmatrix} \cdot \begin{bmatrix} \cos \phi_{a/b} \\ \sin \phi_{a/b} \end{bmatrix} + W_{radial}(\phi_{1,b} + \theta_i) - E_{radial,XY}(\phi_{a/b}) \quad (1)$$

In the equations of the different tests, $r_j(C_i)$ describes the measured radius of Test j at the rotation angle C_i and respectively $r_j(\theta_i)$ specify the radius at the angular position θ_i . The angle $\phi_{a/b}$ describes the angular position of the touch trigger probe during Test 1a and Test 1b. In contrast, the measured values of Test 2 are only influenced by the workpiece related errors and the positioning errors of the linear axes in radial direction at the different measurement positions. The corresponding mathematical relation is shown in Equation (2).

$$r_2(\theta_i) - r_2(0^\circ) = -E_{radial,XY}(\theta_i) + W_{radial}(\theta_i) \quad (2)$$

In Test 3, the measured values depend only on the rotary axis and linear axes related errors, because the touch trigger probe always measure the same point of the workpiece. Equation (3) presents the mathematical description of Test 3.

$$r_3(C_i) - r_3(0^\circ) = \begin{bmatrix} E_{XC,total}(C_i) \\ E_{YC,total}(C_i) \end{bmatrix} \cdot \begin{bmatrix} \cos C_i \\ \sin C_i \end{bmatrix} - E_{radial,XY}(-\theta_i) \quad (3)$$

The mathematical model of the self-calibration approach is established by consolidating the equations of the four tests at the considered angular positions to a system of equations. At each of the N considered angular positions ($i = 1, \dots, N$ for Eqs. (1) to (3)) one equation is generated for each of the four tests. The difference between the measured radii and the reference radius can

be expressed as a linear function of the four error variables at all N considered angular positions. The combination of Eqs. (1) to (3) for $i = 1, \dots, N$ can be written in the form shown in Eq. (4), where the A matrix has the size of $4N \times 4N$.

$$\begin{bmatrix} \Delta r_{1a}(C_1) \\ \Delta r_{1b}(C_1) \\ \Delta r_2(\theta_1) \\ \Delta r_3(C_1) \\ \vdots \\ \Delta r_{1a}(C_N) \\ \Delta r_{1b}(C_N) \\ \Delta r_2(\theta_N) \\ \Delta r_3(C_N) \\ E_{YC,total}(C_i) \end{bmatrix} = \underline{\underline{A}} \cdot \begin{bmatrix} E_{XC,total}(C_1) \\ E_{YC,total}(C_1) \\ E_{radial,XY}(\theta_1) \\ W_{radial}(\theta_1) \\ \vdots \\ E_{XC,total}(C_N) \\ E_{YC,total}(C_N) \\ E_{radial,XY}(\theta_N) \\ W_{radial}(\theta_N) \end{bmatrix} \quad (4)$$

As an example, in the experimental case study presented in Section 3, eight rotation angles respectively measurement positions between 0° and 360° in steps of 45° are considered. Consequently, $N = 8$ and $\underline{\underline{A}}$ has the size 32×32 . However, the matrix does not have full rank and therefore the following boundary conditions have to be defined to ensure the solvability of the mathematical model.

- 1) $E_{XC,total}(0^\circ) = E_{YC,total}(0^\circ) = E_{radial,XY}(0^\circ) = W_{radial}(0^\circ) = 0$
All the errors are defined with respect to the initial angle $C_i = 0$ or $\theta_i = 0$.
- 2) $E_{radial,XY}(90^\circ) = E_{radial,XY}(-90^\circ)$
This does not result in any information loss, because it only defines the reference in the Y-direction.
- 3) $E_{radial,XY}(0^\circ) = E_{radial,XY}(180^\circ)$
This constraint, in addition to 1), assumes that there is no positioning error along the X axis. This leads to a limitation of the proposed self-calibration approach. This constraint is needed because it is not mathematically possible to get the absolute value of $E_{radial,XY}(180^\circ)$ out of the proposed self-calibration scheme. The proposed scheme can only estimate the linear positioning error of Y-axis relative to the X-axis. If the linear positioning error of X-axis needs to be calibrated, a direct measurement can be for example realized by a length artefact which is measured by the touch trigger probe.

In consideration of these boundary conditions, the mathematical model of the self-calibration approach includes 26 unknown variables and becomes solvable for $N = 8$.

Table 2 Machine tool specifications.

Stroke	X: 500 mm, Y: 350 mm, Z: 510 mm, B: +160 - +180°; C: 360°
Resolution	X, Y, Z: 0.001 mm, B,C: 0.001°

Table 3 Touch trigger probe specifications (Renishaw OMP400).

Sense direction	$\pm X, \pm Y, \pm Z$
Repeatability (2σ)	0.35 μm
Stylus length	100mm

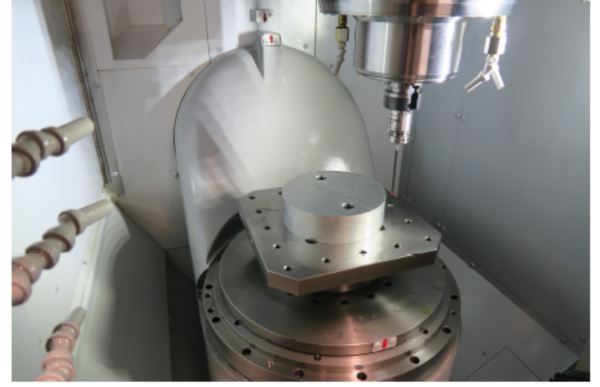
3 Experimental Case Study

3.1 Experimental Setup

The presented self-calibration approach is applied to a commercial mid-size five-axis machine tool, which is shown in Figure 2. The rotary axis and the swiveling axis are arranged on the workpiece side and the linear axes on the tool side. According to ISO 10791-2 [1] the kinematic chain of the machine tool is described as follows: $V[w - C - B - b - Y - X - Z - (C) - t]$. The relevant characteristics of the machine tool are summarized in Table 2. Furthermore, the high accuracy touch trigger probe OMP400 by Renishaw is used for the experiments. This touch trigger probe is recommended for process setting, in-process control and post-process monitoring and thus provides good characteristics for the usage in the self-calibration approach. The radial offsets of the stylus sphere from the spindle axis was calibrated before the experiments. The characteristics of this touch trigger probe are listed in Table 3. In the experimental case study, a workpiece with a diameter of about 90 mm is employed. The corresponding experimental setup is shown in Figure 3. The workpiece is fixed on the machine tool table by two screws.

3.2 Measurement results

The eight measurement positions, which are spread over the circumference of the workpiece in steps of 45° , result in a total cycle time of about 6 minutes and 30 seconds for the complete test sequence. The difference between the target positions and the measured positions are used to calculate the defined error variables by using the mathematical model presented in Eq. 4. The resulting four error variables $E_{XC,total}(C_i)$, $E_{YC,total}(C_i)$, $E_{radial,XY}(\theta_i)$ and $W_{radial}(C_i)$ are presented in Figure 4. The results show that $W_{radial}(\theta_i)$ is the dominant error among the considered error sources. The maximum value of the measured workpiece related errors $W_{radial}(\theta_i)$ is 76.6 μm . Consequently, compared to

**Fig. 3** Experimental setup of the self-calibration approach.**Table 4** Position errors of the C-axis under investigation detected by the self-calibration approach.

	Value [μm]
E_{X0C}	3.0
E_{Y0C}	5.10

$E_{XC,total}(C_i)$ and $E_{YC,total}(C_i)$ the workpiece related errors are 7 times higher. The positioning errors of the linear axes have the smallest contribution to the total deviations. The maximal positioning error of the linear axes in radial direction identified by the self-calibration approach is $E_{radial,XY}(-135^\circ) = 2 \mu\text{m}$. Furthermore, the profile of $E_{radial,XY}(\theta_i)$ shows the largest errors at the two angular positions $\theta_i = -135^\circ$ and $\theta_i = 45^\circ$. This indicates that the positioning error in radial direction is larger in the first and third quadrant. This suggests a squareness error between the X- and Y-axis.

The position errors E_{X0C} and E_{Y0C} of the rotary axis and the actual radial error motions E_{XC} and E_{YC} are determined by a Gauss circle fit according to ISO 230-7 [2] to realize a more detailed analysis of the C-axis performance. Figure 5 shows the resulting Gauss circle fit and the resulting position errors of the rotary axis. The exact values of the position errors E_{X0C} and E_{Y0C} are given in Table 4. Compared to the position errors, the radial error motions E_{XC} and E_{YC} , which are presented in Figure 6, are significantly smaller. The detected values of E_{XC} and E_{YC} are smaller than the linear axis' resolution of the machine tool. Analysing the machine tool related errors, the position errors of the rotary axis are the dominant errors in the scope of the considered error variables.

4 Uncertainty Analysis

This section discusses the output's uncertainties of the proposed self-calibration approach. The self-calibration

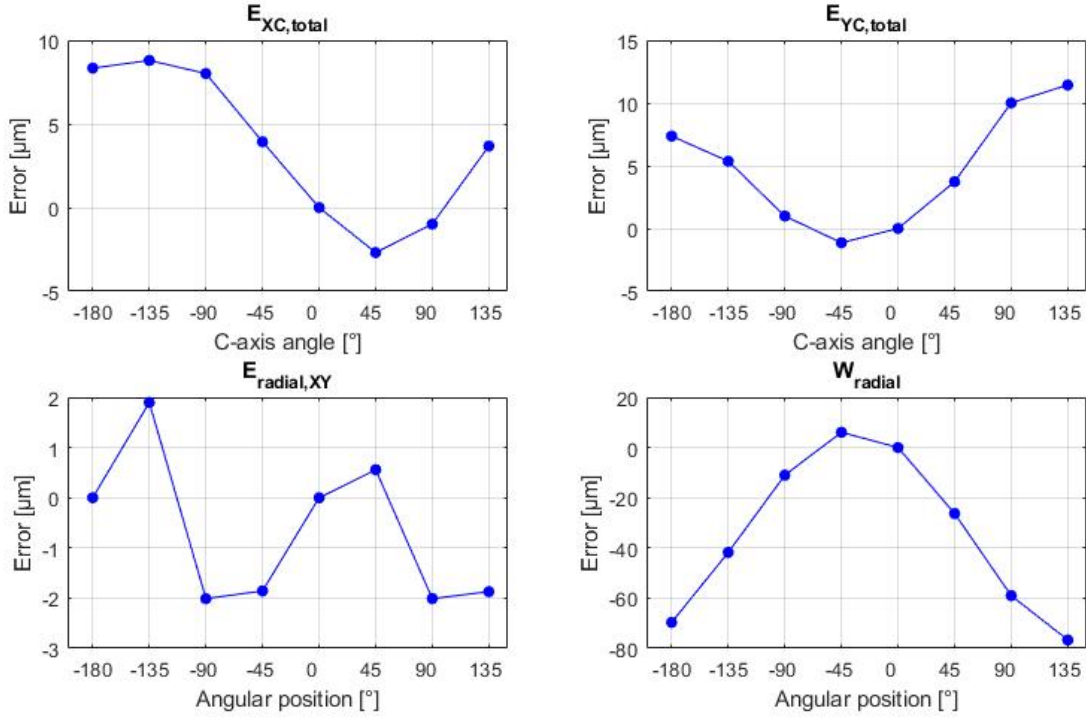


Fig. 4 Resulting values of the error variables identified with the self-calibration approach. a) , b) , c) , d) .

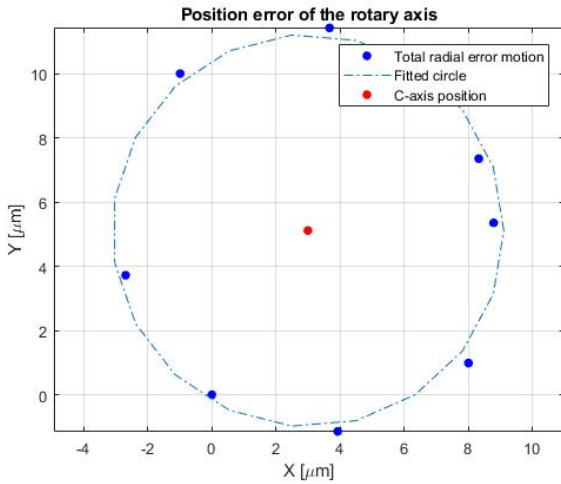


Fig. 5 Position of the C-axis (red dot) identified by the self-calibration approach and least square fitting.

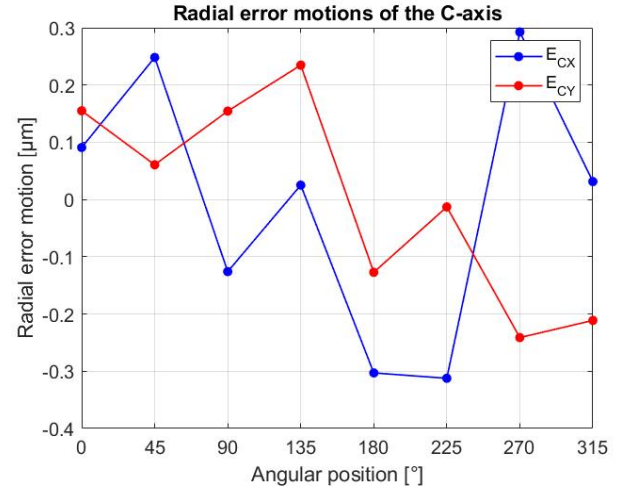


Fig. 6 Actual radial error motions of the C-axis under investigation.

approach is based on a multi-input and multi-output model so that the uncertainty propagation within the model has to be analysed. Following the GUM Uncertainty Framework [14], the Monte Carlo method is used to estimate the uncertainties of the output parameters. In contrast to other indirect calibration approaches for rotary axes, this self-calibration approach includes the influence of the linear axes. Therefore, the uncertainty analysis concentrates on the repeatability of the whole

probing system and the error propagation within the mathematical model of the self-calibration approach.

First, the probability density functions of the input variables are estimated by using the procedure of uncertainty Type A according to [14]. This allows to estimate the repeatability of the complete probing system consisting of the touch trigger probe as well as the machine tool, because the uncertainty Type A is estimated experimentally. The described procedure ex-

Table 5 Expanded uncertainties ($k=2$) of the error variables of the self-calibration approach estimated by the Monte Carlo method with 1 million runs.

	$E_{XC,total}$ [μm]	$E_{YC,total}$ [μm]	$E_{radial,XY}$ [μm]	W_{radial} [μm]
-180°	1.72	6.68	0.0	1.94
-135°	4.07	4.41	3.26	3.71
-90°	4.01	3.44	3.04	3.28
-45°	3.48	4.71	3.19	2.75
45°	2.19	4.10	1.76	1.96
90°	3.49	3.28	3.04	3.09
135°	5.07	6.19	4.60	4.61

Table 6 Expanded uncertainties ($k = 2$) of the error variables of the self-calibration approach estimated by the Monte Carlo method with 1 million runs.

Error variable	Expanded uncertainty ($k = 2$)
E_{X0C} [μm]	3.68
E_{Y0C} [μm]	3.10

ceeds the pure probe repeatability defined in the supplier's handbook. The other factors contributing to the measurement performance such as feed speed, acceleration during the measurement, time delay between the probing signal, and the read-out of the machine tool position are also included in the experimental data if the self-calibration approach is repeated several times. The self-calibration approach is repeated 30 times in order to determine the measurement uncertainty Type A. The systematic error of the thermal drift is removed from the measurement data because in total approximately six hours are required to conduct the 30 repetitions. The maximum standard uncertainty of the 30 repetitions is about $0.9 \mu\text{m}$. Therefore, the calculated uncertainty Type A is smaller than the minimum machine tool resolution, which is $1 \mu\text{m}$. Consequently, the machine tool resolution of $1 \mu\text{m}$ is taken as uncertainty for the input quantities in the Monte Carlo method. In order to estimate the uncertainty of the output quantities a Monte Carlo method with 1 million runs is used to determine the standard uncertainty of the output quantities. Table 5 presents the uncertainties of the error variables at the considered angular positions with a confidence level of 95 % ($k = 2$). The resulting expanded uncertainties of the different output variables are between $2 \mu\text{m}$ and $7 \mu\text{m}$. Furthermore, the resulting uncertainties of the estimated position errors of the C-axis are analysed. The expanded uncertainties of position errors E_{X0C} and E_{Y0C} are listed in Table 6.

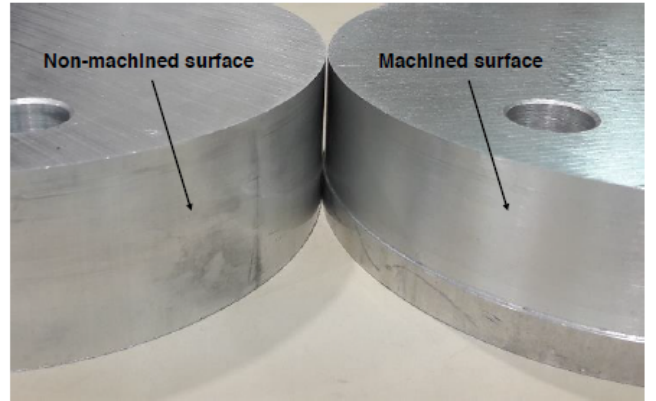


Fig. 7 Comparison between the surface of the non-machined and the machined workpiece.

5 Experimental evaluation of the self-calibration approach

This section experimentally evaluates the performance of the self-calibration approach regarding its error separation capabilities. In each section, a specific error type is investigated in detail. First, the influence of different workpieces and workpiece positions on the results of the self-calibration approach is discussed. Afterwards the position errors of the C-axis are enlarged by shifting the machine tool related coordinate system in different direction and analysing the corresponding results of the self-calibration approach. For a final evaluation, the rotary table position errors identified by the self-calibration approach are compared to that measured by the R-Test. The experimental evaluation analyses if the error separation between the artefact related errors and the geometrical errors of the machine tool is reliable.

5.1 Influence of the workpiece

The dependence of the calibration results on the used measurement artefact is investigated by using two different workpieces. For this comparison, a workpiece with a machined and a workpiece with a non-machined circumference are used for the self-calibration approach. The machined workpiece is the same as in the experimental case study presented in Section 3.2. The circumference of the machined artefact is processed by a turning machine. Figure 7 shows the surfaces of the two measurement artefacts.

Both workpieces have a radius of approximately 90 mm and are cylinders made of aluminium alloy. First, the self-calibration approach is conducted using the cylinder with the non-machined surface and afterwards us-

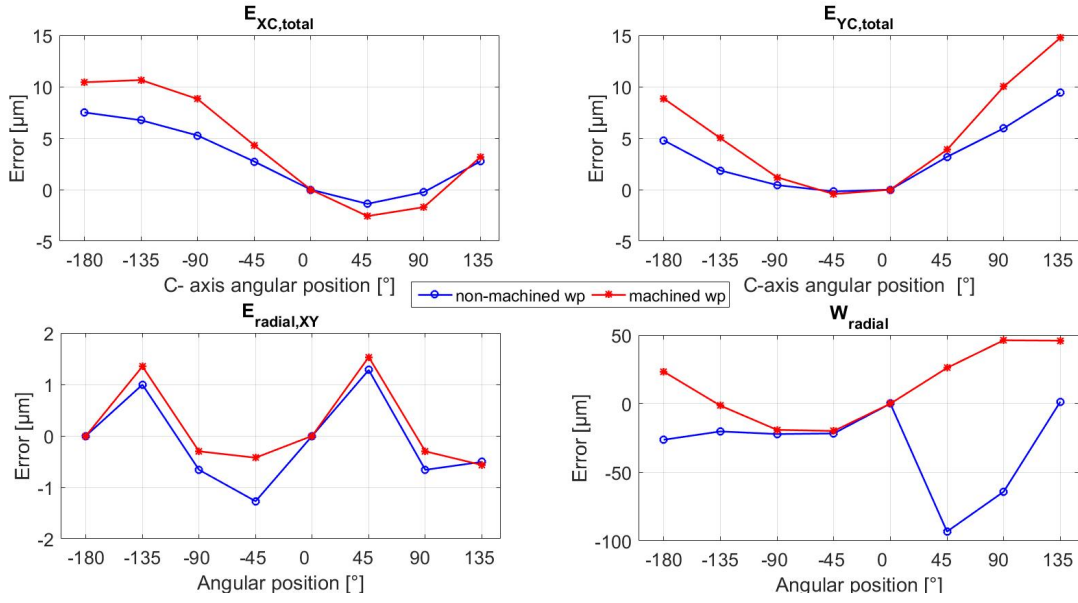


Fig. 8 Comparison of the error variables detected by the self-calibration approach using a machined and a non-machined workpiece.

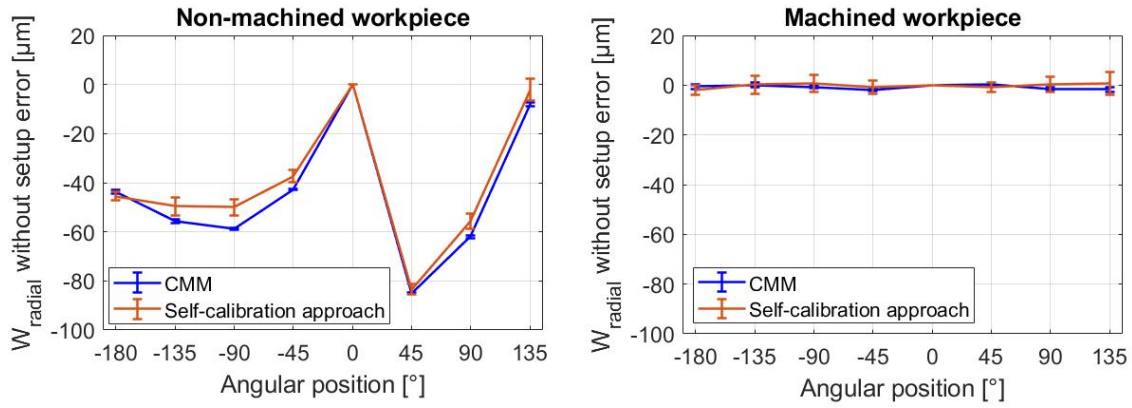


Fig. 9 Comparison of the error $W_{radial}(\theta_i)$ without the influence of the setup error identified by the self-calibration approach and CMM measurements. The error bars of the self-calibration approach indicate the uncertainties ($k=2$) from uncertainty analysis in Section 4 and the error bars of the CMM measurements indicate the uncertainties ($k=2$) resulting from 3 repetitions of the measurements.

ing the workpiece with the machined surface. The self-calibration measurement cycle is repeated ten times per workpiece and the geometrical errors are calculated from the average of those ten measurements to reduce the influence of random effects in the measurements. Figure 8 illustrates the results of both measurement campaigns. This evaluation demonstrates that the identified workpiece errors $W_{radial}(\theta_i)$ differ significantly for the two runs. $W_{radial}(\theta_i)$ of the machined surface indicates mainly a position error of the workpiece relative to the defined coordinate system. However, the non-machined workpiece has additionally large shape deviations for example at $\theta_i = 45^\circ$.

To verify these results, the workpiece related errors identified by the self-calibration approach are compared

to coordinate measurement machine measurements of the two workpieces. The influence of the setup error, which is included in the error $W_{radial}(\theta_i)$, is eliminated so that the results can be compared to the CMM measurements. Figure 9 illustrates the shape deviations of the non-machined and machined workpiece for the self-calibration approach and the CMM measurements. The results of the non-machined workpiece show qualitatively similar shape errors. However, there are numerical difference between the self-calibration and CMM measurements due to the influence of the rough surface of the non-machined workpiece. Consequently, slightly different measurement positions of the touch trigger probe during the self-calibration approach and CMM measurements can result in different measurement val-

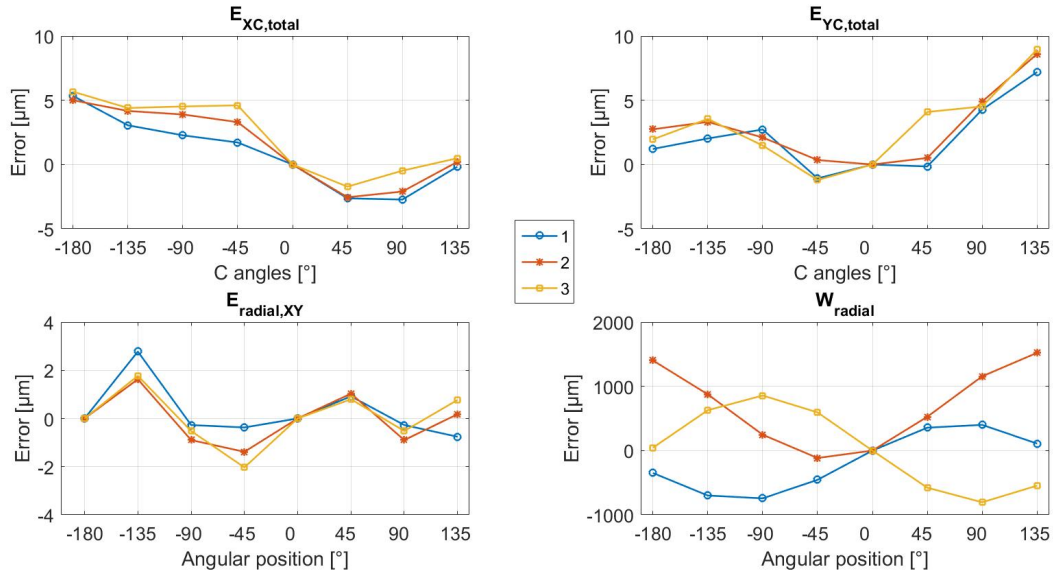


Fig. 10 Identified geometrical errors for different workpiece positions.

Table 7 Comparison of the position errors of the C-axis using a machined and a non-machined workpiece.

	Non-machined surface	Machined surface
E_{X0C} [μm]	3.0	3.9
E_{Y0C} [μm]	4.3	6.8

ues. In the case of the machined workpiece there are no significant shape deviation and the results of the self-calibration approach and the CMM measurements correspond to each other.

The error variable $E_{radial,XY}(\theta_i)$ shows related behaviour for both measuring campaigns. The maximum difference between the determined values for $E_{radial,XY}(\theta_i)$ is 1 μm at the angular position $\theta_i = -45^\circ$. However, $E_{XC,total}(C_i)$ and $E_{YC,total}(C_i)$ show more significant deviations between the two measuring campaigns although the underlying error sources do not depend on the workpiece. The resulting position errors of the C-axis for both measurement artefacts are summarized in Table 7.

However, the thermal drift of the C-axis position can explain the difference between the values of the position errors in both cases. The results visualize that the C-axis position drifts into positive X- and Y direction during the experiments. Thus, the detected C-axis' position errors for the non-machined surface are smaller because the measurements are conducted first. The same drift of the rotary axis position is also observed during the 30 repetitions of the self-calibration, which are conducted for the uncertainty analysis in Section 3 using only the workpiece with the machined surface. The correspond-

Table 8 Identified position errors of the C-axis in the 10th and 20th measurement of the self-calibration approach using the machined workpiece if the self-calibration approach is successively repeated.

	10 th repetition	20 th repetition
E_{X0C} [μm]	2.70	2.97
E_{Y0C} [μm]	3.31	5.44

ing position errors of the C-axis in the 10th and 20th measurement are given in Table 8, which also indicates a thermal drift into the Y direction.

The next analysis investigates the accuracy of the geometrical machine tool errors without aligning the workpiece to the rotary axis using a dial gauge. This experiment uses the workpiece with the machined surface. The workpiece is shifted in different directions to the maximum deviation allowed by the play of the holes. The three test cycles are carried out directly after each other to minimize the thermal influence on the measurement results. Figure 10 presents the determined error variables of this evaluation. The results indicate that W_{radial} is up to 1.5 mm. This is due to the huge position deviations of the workpiece during the experiments. However, the resulting geometrical errors of the machine tool are consistent with each other despite the large position deviation of the workpiece. For instance, the maximum deviation between $E_{XC,total}(C_i)$ of the different workpiece positions is 3 μm and between $E_{YC,total}(C_i)$, it is 4 μm. For $E_{radial,XY}(\theta_i)$ the maximum difference is 2 μm at $\theta_i = -45^\circ$. Thus, the variation of the machine tool related error variables is

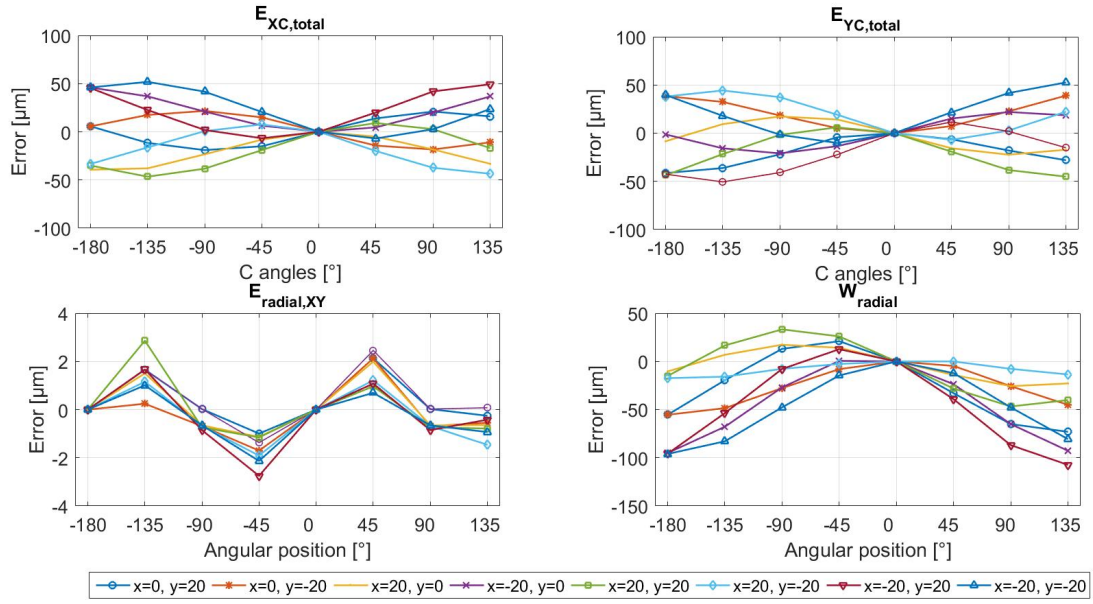


Fig. 11 Error variables identified by the self-calibration approach for different shifted origins. The colors indicate the x and y coordinate in microns.

only within the range of the measurement uncertainties. The results suggest that even if the workpiece has a significantly non-concentric position, the self-calibration algorithm detects the correct machine tool errors. This results in a time reduction of the calibration process and consequently in a decreased downtime of the machine tool, since no time-consuming alignment is required.

5.2 Accuracy of the C-axis position estimation

This subsection assesses the results of the self-calibration approach for larger C-axis position errors. The measurement results in subsection 3.2 shows that the geometrical errors of the machine tool under investigation are small compared to the measurement uncertainties of the self-calibration approach. In order to imitate larger C-axis position errors the origin of the machine coordinate system used in the measurements is shifted to different locations. It is expected that the radial positioning errors of linear axes do not change significantly within this experiment, because the coordinate system is only shifted by few micrometres. The shift of the coordinate systems relative to the initial origin causes position errors of the C-axis as well as of the workpiece in the new coordinate system. In total, eight different origins of the coordinate system are analysed by conducting the self-calibration approach. The origins are located on a square with the side length of 40 μm around the initial origin. The corresponding results of the self-calibration approach are presented in Figure 11.

Figure 11 indicates that the induced behaviour of $E_{XC,total}(C_i)$, $E_{YC,total}(C_i)$ and $W_{radial}(\theta_i)$ is correctly identified by the self-calibration algorithm, because the error variables incorporate the shifts of the origin. Furthermore, the radial positioning errors of the linear axes differ only slightly between the implemented origins. The maximum difference between the radial positioning errors at the same angular position is about 3 μm . The detected position errors of C-axis for the different origins are summarized in Table 9.

To evaluate W_{radial} identified by the different measurements in Figure 11, the additional eccentricities resulting from the shift of the coordinate system are eliminated from the measurement data to compare the measured real setup errors. Figure 12 indicates that the workpiece related errors identified by the self-calibration approach are reproducible for the eight measurements within the expanded uncertainties except for one outlier. This experiment clarify that the self-calibration al-

Table 9 Position errors of the C-axis in the different coordinate systems.

Origin position [μm]	E_{X0C} [μm]	E_{Y0C} [μm]
x=0, y=20	-0.17	-20.08
x=0, y=-20	1.06	20.40
x=20, y=0	-20.25	-2.06
x=-20, y=0	22.83	1.07
x=20, y=20	-18.70	-20.38
x=20, y=-20	-17.58	18.69
x=-20, y=20	22.43	-20.19
x=-20, y=-20	22.53	20.83

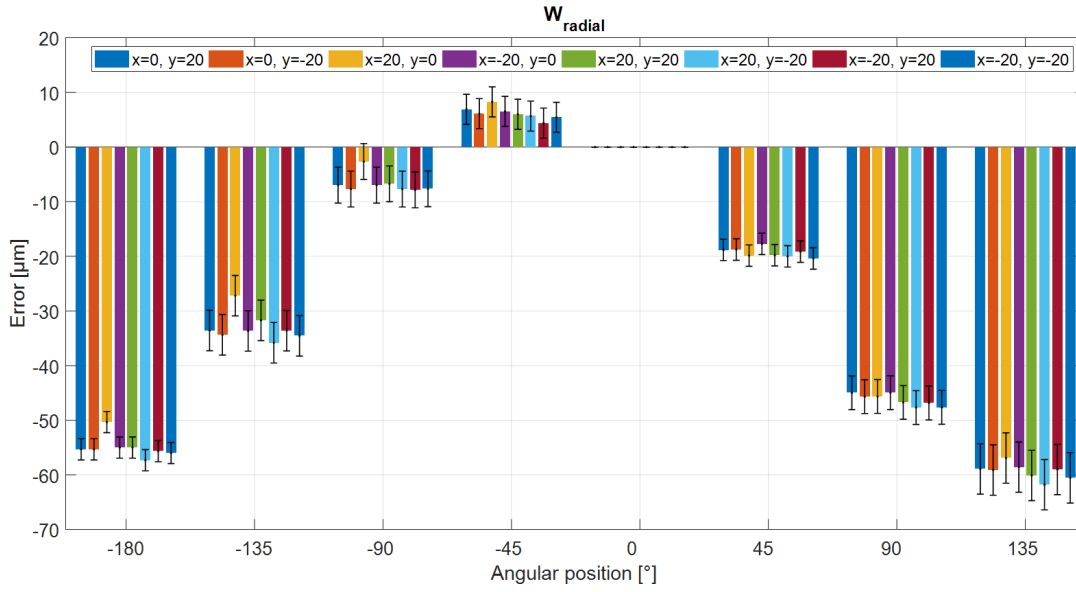


Fig. 12 Identified error variables $W_{radial}(\theta_i)$ with the corresponding expanded uncertainties ($k=2$) of the measurements after eliminating the influence of the additional eccentricities caused due to the shift of the coordinate system.

gorithm can reliably detect the implemented position errors of the workpiece and the rotary axis within the range of the measurement uncertainty.

5.3 Comparing the self-calibration approach to the adapted R-Test

The final evaluation compares the results of the self-calibration approach to the results of an established measurement method. In order to measure the total radial error motions of the rotary axis an adapted R-Test is used. The setup of the adapted R-Test consists of a precision sphere, which is mounted into the tool holder of the machine tool, and a sensor nest containing three displacement sensors fixed on the rotary table. The experimental setup of the adapted R-Test is shown in Figure 13.

The sensor nest of the adapted R-Test is mounted in the centre of the rotary table instead of an eccentric position as in the conventional R-Test. The spindle is placed at the nominal position of the C-axis. Afterwards the sphere displacement is measured by the adapted R-Test discretely with the same rotation angles as the self-calibration approach. In the conventional R-Test setup, where the sensor nest has an eccentric position, the measurement would be influenced by a rotary axis and linear axes. In this setup, the influence of the linear axes errors is avoided, which allows a direct comparison of the rotary axis error motions, identified by the proposed self-calibration approach, with the one measured by the R-Test. Figure 13 compares the total radial error

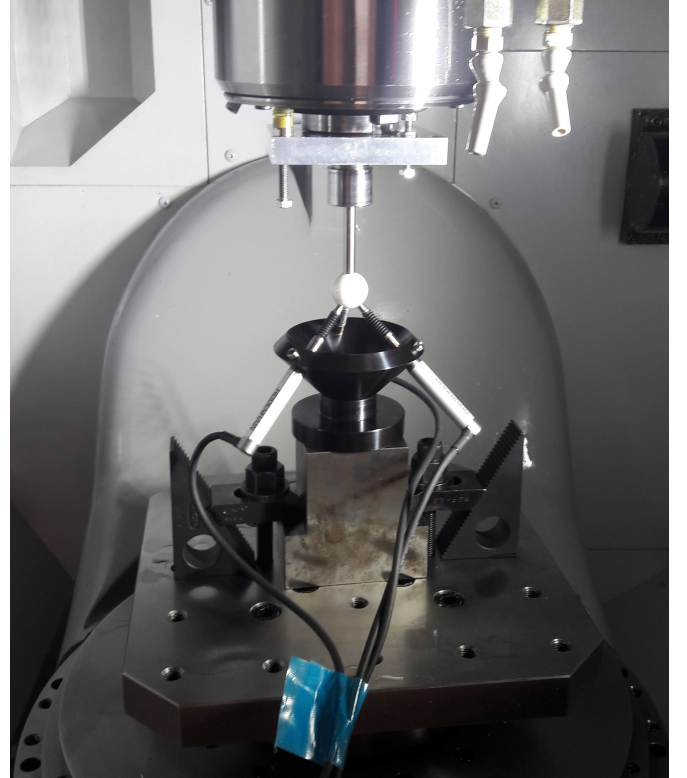


Fig. 13 Experimental setup of the adapted R-Test discrete.

motions $E_{XC,total}(C_i)$ and $E_{YC,total}(C_i)$, measured by the adapted R-Test and the self-calibration approach including the corresponding uncertainties. The uncertainties of the self-calibration approach are estimated by the uncertainty analysis presented in Section 4. Geb-

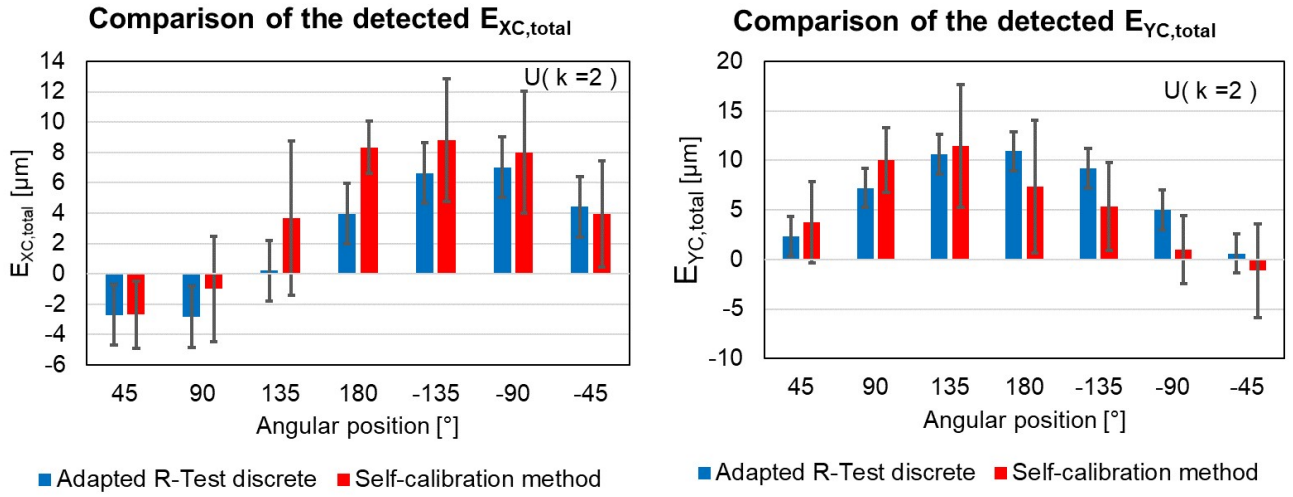


Fig. 14 Comparison of the total radial error motions measured by the adapted R-Test and self-calibration method.

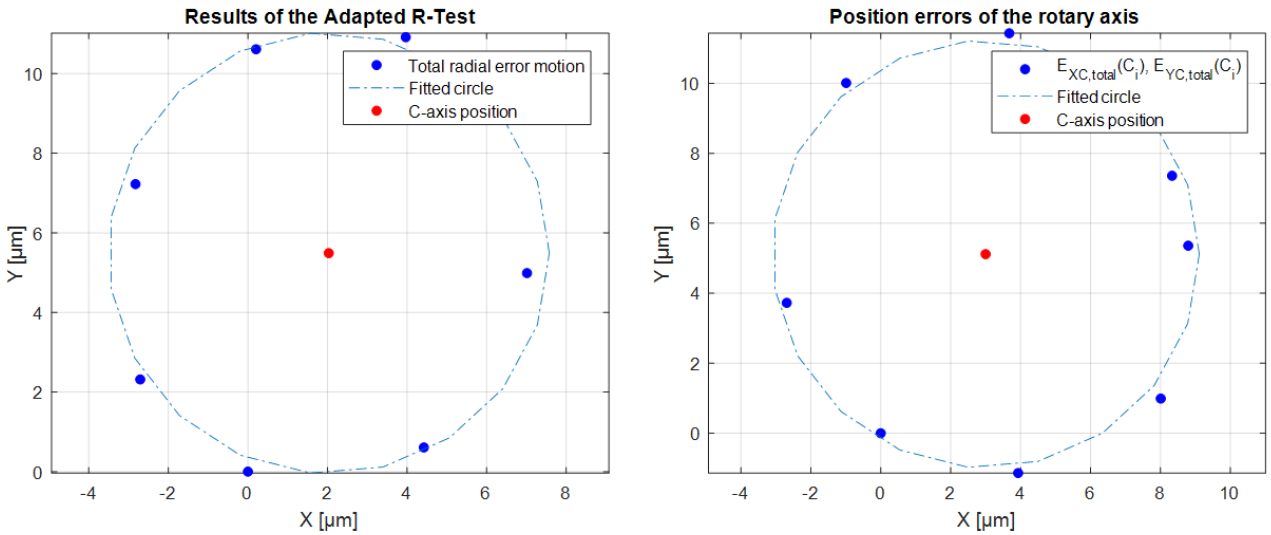


Fig. 15 Comparison of the C-axis' position errors detected by the adapted R-Test discrete and the self-calibration approach.

hard [8] estimates the expanded uncertainty of the R-Test as $\pm 2 \mu\text{m}$. Consequently, the results of the adapted R-Test discrete have a lower uncertainty than the results of the self-calibration approach.

Figure 14 shows that the results for the total radial error motions in X- and Y- direction identified by the adapted R-Test and the self-calibration approach are consistent. The maximum deviation between the results of the adapted R-Test discrete and the self-calibration algorithm is $4 \mu\text{m}$ for $E_{XC,total}(180^\circ)$. Considering $E_{YC,total}$, the maximum difference between the two methods is also about $4 \mu\text{m}$ at -90° and -135° . Only for the error variables $E_{YC,total}(180^\circ)$ there is no overlapping of the expanded uncertainty intervals. In conclusion, the self-calibration approach delivers accurate results compared to the adapted R-Test. Therefore, it is a suitable approach to detect $E_{YC,total}(C_i)$ and

Table 10 Comparison of the position errors identified by the self-calibration approach and the adapted R-Test.

	$E_{X0C} [\mu\text{m}]$	$E_{Y0C} [\mu\text{m}]$
Self-calibration approach	3.00	5.00
R- Test discrete	2.00	5.50

$E_{XC,total}(C_i)$. Figure 15 presents the resulting position errors E_{C0X} and E_{C0Y} measured by the self-calibration approach and the adapted R-Test.

Table 10 compares the position errors of the C-axis average line determined by the adapted R-Test and the self-calibration approach. The maximal difference of the C-axis position errors detected by the two approaches is $1 \mu\text{m}$. This comparison shows that the self-calibration approach and the adapted R- Test detect comparable

position errors of the C-axis under investigation. In contrast to the adapted R-Test the self-calibration approach does not require a complicated measurement setup to identify these position errors. However, the simplification of the measurement setup results in an increased expanded uncertainty of the self-calibration approach compared to the adapted R-Test. The expanded uncertainty of the self-calibration approach depends on the repeatability characteristics and resolution of the linear scales of the machine tool. Thus, the expanded uncertainty can be further reduced for machine tools with a higher resolution of the linear scales.

6 Conclusion

The presented self-calibration approach enables the complete error separation in radial direction between two linear axes, one rotary axis and the errors of an uncalibrated cylindrical artefact used in the measurement cycle. Thus, the self-calibration approach considers all relevant error source to detect the radial error motions as well as the position error of a rotary axis, in contrast to many other on-machine measurement cycles, which often neglect the influence of the linear axes on the calibration result of the rotary axis. Furthermore, the self-calibration approach provides an efficient and automatic calibration procedure for a rotary axis parallel to the spindle by using a touch trigger probe and an uncalibrated artefact. In contrast to conventional calibration schemes, no double ball bar setup or precision sphere and linear displacement sensors are needed. This results in a decreased downtime of the machine tool during the calibration process because no specific measurement setup has to be installed. The validity of the self-calibration approach is investigated by a series of experiments. This evaluation shows that neither the used artefact nor the position of the artefact have a significant influence on the machine tool errors identified by the self-calibration approach. Additionally, the calculated errors obtained from the self-calibration approach are compared to the results of an adapted R-Test discrete. The self-calibration approach obtains an accuracy comparable to the adapted R-Test discrete without requiring the complicated measurement setup. The uncertainty analysis shows that the expanded uncertainty ($k = 2$) of the identified geometrical errors is maximum 7 μm . In conclusion, the proposed self-calibration can be used as automated calibration procedure for rotary axes and linear axes of machine tools with large geometrical errors.

Acknowledgements The authors would like to thank Prof. Konrad Wegener, Prof. Atsushi Matsubara and Dr. Josef Mayr for their support.

Conflict of interest

The authors declare that they have no conflict of interest.

References

1. ISO 10791-2. Test conditions for machining centres – part 2: geometric tests for machines with vertical spindle or universal heads with vertical primary rotary axis (vertical Z-axis). Geneva, Switzerland: International Organization for Standardization ISO.
2. ISO 230-7:2015, Test Code for Machine Tools — Part 3: Geometric accuracy of axes of rotation, International Organization for Standardization ISO, Geneva, Switzerland.
3. Bringmann, B., Knapp, W.: Model-based 'Chase-the-Ball' calibration of a 5-axes machining center. *CIRP Annals - Manufacturing Technology* **55**(1), 531–534 (2006). DOI 10.1016/S0007-8506(07)60475-2
4. Bringmann, B., Knapp, W.: Machine tool calibration: Geometric test uncertainty depends on machine tool performance. *Precision Engineering* **33**(4), 524–529 (2009). DOI 10.1016/j.precisioneng.2009.02.002
5. Erkan, T., Mayer, J.R.R., Dupont, Y.: Volumetric distortion assessment of a five-axis machine by probing a 3D reconfigurable uncalibrated master ball artefact. *Precision Engineering* **35**(1), 116–125 (2011). DOI 10.1016/j.precisioneng.2010.08.003. URL <http://dx.doi.org/10.1016/j.precisioneng.2010.08.003>
6. Evans, C.J., Hocken, R.J., Estler, W.T.: Self-Calibration: Reversal, Redundancy, Error Separation, and 'Absolute Testing'. *CIRP Annals - Manufacturing Technology* **45**(2), 617–634 (1996). DOI 10.1016/S0007-8506(07)60515-0
7. Gao, W., Kiyono, S., Sugawara, T.: High-accuracy roundness measurement by a new error separation method. *Precision Engineering* **21**(97), 123–133 (1997). DOI 10.1016/S0141-6359(97)00081-0
8. Gebhardt, M.: Thermal behaviour and compensation of rotary axes in 5-axis machine tools. ETH Zurich (2014)
9. Guenther, A., Stöbener, D., Goch, G.: Self-Calibration Method for a Ball Plate Artefact on a CMM. *CIRP Annals - Manufacturing Technology* **65**(1), 503–506 (2016). DOI 10.1016/j.cirp.2016.04.080
10. Ibaraki, S., Iritani, T., Matsushita, T.: Calibration of location errors of rotary axes on five-axis machine tools by on-the-machine measurement using a touch-trigger probe. *International Journal of Machine Tools and Manufacture* **58**, 44–53 (2012). DOI 10.1016/j.ijmachtools.2012.03.002. URL <http://dx.doi.org/10.1016/j.ijmachtools.2012.03.002>
11. Ibaraki, S., Ota, Y.: Error map construction for rotary axes on five-axis machine tools by on-the-machine measurement using a touch-trigger probe. *International Journal of Automation Technology* **8**(1), 20–27 (2013). DOI 10.1016/j.ijmachtools.2013.01.001. URL <http://dx.doi.org/10.1016/j.ijmachtools.2013.01.001>

12. Ibaraki, S., Ota, Y.: A machining test to evaluate geometric errors of five-axis machine tools with its application to thermal deformation test. *Procedia CIRP* **14**, 323–328 (2014). DOI 10.1016/j.procir.2014.03.109. URL <http://dx.doi.org/10.1016/j.procir.2014.03.109>
13. Ibaraki, Soichi; Knapp, W.: Indirect Measurement of Volumetric Accuracy for Three-Axis and Five-Axis Machine Tools A Review **44**(23) (2015). DOI 10.3929/ETHZ-B-000225616
14. JCGM: Evaluation of measurement data—guide to the expression of uncertainty in measurement. *Int. Organ. Stand. Geneva* **50**, 134 (2008)
15. Kniel, K., Härtig, F., Osawa, S., Sato, O.: Two highly accurate methods for pitch calibration. *Measurement Science and Technology* **20**(11) (2009). DOI 10.1088/0957-0233/20/11/115110
16. Lee, K.I., Yang, S.H.: Measurement and verification of position-independent geometric errors of a five-axis machine tool using a double ball-bar. *International Journal of Machine Tools and Manufacture* **70**, 45–52 (2013). DOI 10.1016/j.ijmachtools.2013.03.010. URL <http://dx.doi.org/10.1016/j.ijmachtools.2013.03.010>
17. Lu, X., Jamalain, A.: A new method for characterizing axis of rotation radial error motion: Part 1. Two-dimensional radial error motion theory. *Precision Engineering* **35**(1), 73–94 (2011). DOI 10.1016/j.precisioneng.2010.08.005. URL <http://dx.doi.org/10.1016/j.precisioneng.2010.08.005>
18. Lu, X., Jamalain, A., Graetz, R.: A new method for characterizing axis of rotation radial error motion: Part 2. Experimental results. *Precision Engineering* **35**(1), 95–107 (2011). DOI 10.1016/j.precisioneng.2010.08.006. URL <http://dx.doi.org/10.1016/j.precisioneng.2010.08.006>
19. Mayer, J.R.R.: Five-axis machine tool calibration by probing a scale enriched reconfigurable uncalibrated master balls artefact. *CIRP Annals - Manufacturing Technology* **61**(1), 515–518 (2012). DOI 10.1016/j.cirp.2012.03.022. URL <http://dx.doi.org/10.1016/j.cirp.2012.03.022>
20. Mayer, J.R.R., Rahman, M.M., Los, A.: An uncalibrated cylindrical indigenous artefact for measuring inter-axis errors of a five-axis machine tool. *CIRP Annals - Manufacturing Technology* **64**(1), 487–490 (2015). DOI 10.1016/j.cirp.2015.04.015. URL <http://dx.doi.org/10.1016/j.cirp.2015.04.015>
21. Nafi, A., Mayer, J.R.R., Wozniak, A.: Novel CMM-based implementation of the multi-step method for the separation of machine and probe errors. *Precision Engineering* **35**(2), 318–328 (2011). DOI 10.1016/j.precisioneng.2010.11.007. URL <http://dx.doi.org/10.1016/j.precisioneng.2010.11.007>
22. Osawa, S., Busch, K., Franke, M., Schwenke, H.: Multiple orientation technique for the calibration of cylindrical workpieces on CMMs. *Precision Engineering* **29**(1), 56–64 (2005). DOI 10.1016/j.precisioneng.2004.04.006
23. Rahman, M.M., Mayer, J.R.R.: Five axis machine tool volumetric error prediction through an indirect estimation of intra- and inter-axis error parameters by probing facets on a scale enriched uncalibrated indigenous artefact. *Precision Engineering* **40**, 94–105 (2015). DOI 10.1016/j.precisioneng.2014.10.010. URL <http://dx.doi.org/10.1016/j.precisioneng.2014.10.010>
24. Wang, Q., Miller, J., Von Freyberg, A., Steffens, N., Fischer, A., Goch, G.: Error mapping of rotary tables in 4-axis measuring devices using a ball plate artifact. *CIRP Annals* **67**(1), 559–562 (2018). DOI 10.1016/j.cirp.2018.04.005. URL <https://doi.org/10.1016/j.cirp.2018.04.005>
25. Weikert, S., Knapp, W.: R-test, a new device for accuracy measurements on five axis machine tools. *CIRP Annals - Manufacturing Technology* **53**(1), 429–432 (2004). DOI 10.1016/S0007-8506(07)60732-X
26. Wiessner, M., Blaser, P., Böhl, S., Mayr, J., Knapp, W., Wegener, K.: Thermal test piece for 5-axis machine tools. *Precision Engineering* **52**, 407–417 (2018)
27. Xiang, S., Yang, J.: Using a double ball bar to measure 10 position-dependent geometric errors for rotary axes on five-axis machine tools. *International Journal of Advanced Manufacturing Technology* **75**(1-4), 559–572 (2014). DOI 10.1007/s00170-014-6155-2